Available online at www.sciencedirect.com
ScienceDirect
Journal of Power Sources 159 (2006) 193–199
JOURNAL OF POWER SOURCES
www.elsevier.com/locate/jpowsour

All-solid-state lithium secondary batteries using sulfide-based glass–ceramic electrolytes

Masahiro Tatsumisago *, Fuminori Mizuno, Akitoshi Hayashi

Department of Applied Chemistry, Osaka Prefecture University, Sakai, Osaka 599-8531, Japan

Available online 24 May 2006

Abstract

Highly lithium ion conducting glass–ceramics in the system Li_2S–P_2S_5 were successfully prepared by a heat treatment of the mechanochmically prepared sulfide glasses. The $80Li_2S{\cdot}20P_2S_5$ (mol.%) glass–ceramic mainly composed of the crystal analogous to the highly conductive thio-LISICON II phase in the system $Li_{4-x}Ge_{1-x}P_xS_4$ showed conductivity as high as 10^{-3} S cm^{-1} at room temperature. The $70Li_2S{\cdot}30P_2S_5$ glass–ceramic, in which the highly ion conductive new metastable phase was formed on heating, showed the highest conductivity of 3.2×10^{-3} S cm^{-1} and the lowest activation energy of 12 kJ mol^{-1} for conduction. The all-solid-state battery In/$80Li_2S{\cdot}20P_2S_5$ glass–ceramic/$LiCoO_2$ exhibited excellent cycling performance of over 500 times with no decrease in the charge–discharge capacity (100 mAh g^{-1}).

The SnS–P_2S_5 glasses as active materials were mechanochemically prepared from SnS and P_2S_5. High performance of these glassy electrode materials was observed in the rechargeable cell of $80SnS{\cdot}20P_2S_5$/$80Li_2S{\cdot}20P_2S_5$ glass–ceramic/$LiCoO_2$, in which a continuous sulfide network between electrode and electrolyte was successfully formed.

The effects of conductive additives in composite electrodes on charge–discharge behavior of all-solid-state cells with Li_2S–P_2S_5 glass–ceramics as a solid electrolyte were investigated. Under a current density over 1 mA cm^{-2}, the cell with vapor grown carbon fiber kept larger discharge capacities during 50 cycles than the cell with acetylene black. The design of continuous electron conducting path from a point of view of morphology for conductive additives is important to improve cell performances of all-solid-state lithium secondary batteries.
© 2006 Elsevier B.V. All rights reserved.

Keywords: Solid electrolyte; All-solid-state battery; Glass–ceramics; Sulfide; Electrode

1. Introduction

Much attention has been paid to all-solid-state lithium secondary batteries because the replacement of conventional liquid electrolytes with inorganic solid electrolytes essentially improves safety and reliability of lithium batteries [1,2]. There are two approaches of developing all-solid-state batteries; one is a thin-film battery prepared by RF sputtering and laser ablation, and the other is a bulk-type battery constructed of electrolyte and electrode powders. Several all-solid-state thin film batteries with inorganic glassy electrolytes such as lithium phosphorus oxynitrides (LiPON) have been reported to show excellent long-cycling performances at room temperature [3,4]. The bulk-type battery has an advantage of enhancing cell capacity by the addition of large amounts of active materials to the cell. Both utilizing highly conductive solid electrolytes and achieving a close contact between electrolyte and electrode powders are key to improve the cell performance. Sulfide-based glassy materials are promising solid electrolyte for bulk-type all-solid-state batteries because of their several advantages in comparison with the crystalline solid electrolytes: a higher ion conductivity, a wide range selection of compositions, isotropic properties, no grain boundaries, easy film formation, and so on [5]. The electrochemical performance of all-solid-state In/$LiCoO_2$ cells with the Li_2S–SiS_2–Li_3PO_4 glasses was firstly reported in 1994 by Kondo and co-workers [6] and then this type of cells with sulfide solid electrolytes have been developed [7–12]. In the bulk-type cells a composite electrode composed of electrode active, solid electrolyte, and electron conductive materials has been used to build the conduction pathways of ions and electrons in the electrode parts. The design of the suitable composite electrode is important to improve the properties of this type of all-solid-state batteries, especially high-rate performance.

On the other hand, we have recently discovered a series of highly conductive glass–ceramics in the Li_2S-based sulfide systems, in which superionic metastable phases are formed from

* Corresponding author. Tel.: +81 72 2549331; fax: 81 72 2549913.
E-mail address: tatsu@chem.osakafu-u.ac.jp (M. Tatsumisago).

0378-7753/$ – see front matter © 2006 Elsevier B.V. All rights reserved.
doi:10.1016/j.jpowsour.2006.04.037

the sulfide glasses [13,14]. Superionic phase is sometimes high-temperature or metastable phase and these phases are easily formed from supercooled liquid like in the case of heating glass beyond glass-transition temperature [5]. The formation of these glass–ceramic materials via glass-heating process is thus very promising in the preparation of highly conductive solid electrolytes for all-solid-state batteries.

The present paper reports the preparation and characterization of Li_2S-based glass–ceramic materials in the system Li_2S–P_2S_5. We also report their application to all-solid-state lithium secondary batteries, focusing on three components constructing composite electrodes in the all-solid-state cells: solid electrolyte, electrode material, and conductive additive. The effects of these components, especially Sn-based active materials and electronic conducting additives, on the electrochemical performance of the all-solid-state cells with sulfide solid electrolytes are discussed.

2. Experimental procedure

The Li_2S–P_2S_5 glass–ceramics were prepared by mechanical milling (MM) and subsequent heat treatment. The MM was performed using a planetary ball mill apparatus of Fritsch Pulverisette 7. Alumina pots and balls were mainly used for milling and the rotation speed was about 370 rpm. The obtained glassy samples were pelletized and heated up to various temperatures over their crystallization temperatures to form the glass–ceramic materials. All the processes were carried out in a dry Ar-filled glove box. Electrical conductivities were measured for the glassy and glass–ceramic pellets by the ac impedance method.

In order to construct laboratory-scale solid-state cells, composite electrodes were prepared by mixing three powders of active materials like $LiCoO_2$, solid electrolytes of the prepared glass–ceramics, and electronic conducting materials like acetylene black (AB); in some cases, Sn-based glassy materials were used as an active material, and in the other cases a piece of indium foil was used as a negative electrode. The all-solid-state cells were charged and discharged under a constant current density from 64 to 1280 $\mu A\,cm^{-2}$ at room temperature in an Ar atmosphere.

3. Results and discussion

3.1. Highly conductive glass–ceramics in the system Li_2S–P_2S_5

In general, crystallization of glassy materials is well known to lower conductivities [15]. However, conductivity enhancement was observed by a heat treatment of the mechanochemically prepared Li_2S–P_2S_5 glasses at around their crystallization temperatures [13] while the conductivity of the Li_2S–SiS_2-based glasses drastically decreased with the heat treatment at their crystallization temperatures. The obtained Li_2S–P_2S_5 glass–ceramic materials exhibited ambient temperature conductivity of about $10^{-3}\,S\,cm^{-1}$ in compressed pellet and, therefore, the glass–ceramics are attractive solid electrolytes for all-solid-state lithium secondary batteries.

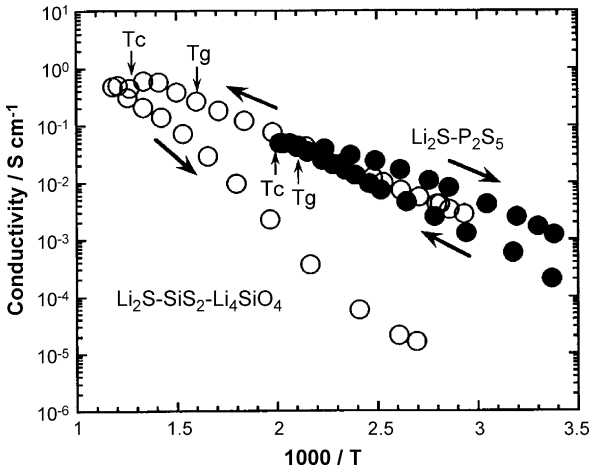

Fig. 1. Temperature dependence of conductivities for the $80Li_2S{\cdot}20P_2S_5$ glass prepared by mechanical milling (closed circles) and the $95(0.6Li_2S{\cdot}0.4SiS_2){\cdot}5Li_4SiO_4$ melt-quenched glass (open circles).

Fig. 1 shows the temperature dependence of conductivities for the $80Li_2S{\cdot}20P_2S_5$ (mol.%) glass prepared by mechanical milling (closed circles) and the $95(0.6Li_2S{\cdot}0.4SiS_2){\cdot}5Li_4SiO_4$ (mol.%) melt-quenched glass (open circles) [16]. The conductivity measurements were carried out on the heating process up to the temperatures beyond their glass transition (T_g) and crystallization temperatures (T_c) and then the cooling process down to ambient temperature in both systems. The crystallization of the Li_2S–SiS_2-based glass decreases conductivity on heating beyond T_c and this behavior is commonly observed in glassy ion conductors. In this case, the decrease in conductivity of the glass is due to the precipitation of Li_4SiS_4 crystal with low conductivity. On the other hand, the conductivity enhancement is observed in the Li_2S–P_2S_5 system after heating at a temperature beyond T_c. In the case of $80Li_2S{\cdot}20P_2S_5$ the conductivities on the cooling process are higher than those on the heating process. The ambient temperature conductivity on the cooling process is $1.3 \times 10^{-3}\,S\,cm^{-1}$, which is almost four times larger than the conductivity of the as-prepared glass. The crystallization occurs during the heating process, and this unexpected phenomenon is explained by the formation of superionic crystalline phases in this system.

The X-ray diffraction patterns of the $80Li_2S{\cdot}20P_2S_5$ samples before and after being heated up to temperatures just above T_c indicated the diffraction pattern after crystallization is very similar to that of the thio-LISICON $Li_{4-x}Ge_{1-x}P_xS_4$ phase in region II ($0.6 < x < 0.8$) (abbreviated name: thio-LISICON II), which was reported to exhibit high conductivity of $2.2 \times 10^{-3}\,S\,cm^{-1}$ at room temperature [17]. Although thio-LISICON $Li_{3+5x}P_{1-x}S_4$ without germanium has also been synthesized by solid phase reaction [18], this thio-LISICON phase is reported to have the different structure from the thio-LISICON II and exhibit lower conductivity of $1.5 \times 10^{-4}\,S\,cm^{-1}$ than the thio-LISICON II and the glass–ceramics. The crystal phases with the same structure as the thio-LISICON II were not formed by solid phase reaction in the Li_2S–P_2S_5 binary system [18], suggesting that the thio-LISICON II analog would be precipitated as a metastable phase from the mechanically milled glass.

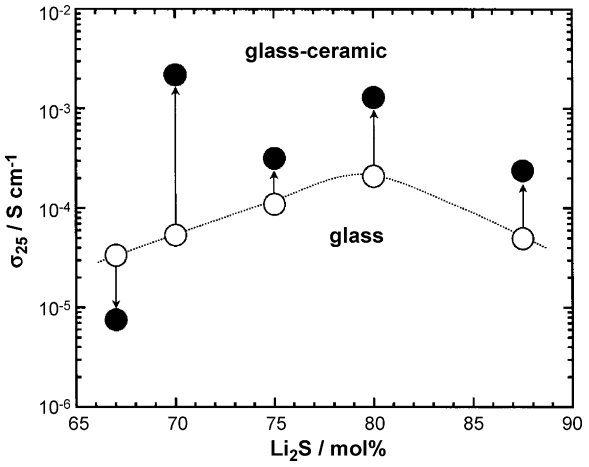

Fig. 2. Composition dependence of ambient temperature conductivity for the glasses in the system Li_2S-P_2S_5 prepared by MM (open circles) and that for the glass–ceramics obtained by the crystallization of these glasses (closed circles).

The crystallization of the thio-LISICON II analog with high conductivity is responsible for the marked enhancement of conductivity in the $80Li_2S{\cdot}20P_2S_5$ glass.

Fig. 2 shows the composition dependence of ambient temperature conductivity for the glasses in the system Li_2S–P_2S_5 prepared by mechanical milling (open circles) and that for the glass–ceramics obtained by the crystallization of these glasses (closed circles). The heat treatment was carried out at temperatures just above T_c. The conductivity of the original glasses increases with an increase in the Li_2S content up to 80 mol.% and it decreases with the addition of Li_2S more than 80 mol.%. The increase of conductivity for the glasses with Li_2S content is due to the increase of ion carrier concentration and the subsequent decrease is due to the precipitation of less conductive Li_2S crystals. Although the conductivity enhancement with crystallization is observed in all the glass compositions with more than 70 mol.%Li_2S, the conductivity difference between glasses and corresponding glass–ceramics depends on the composition. In the case of $80Li_2S{\cdot}20P_2S_5$ composition, a remarkable increase of conductivity is observed due to the formation of the thio-LISICON II analog during the crystallization as mentioned above. In the case of $70Li_2S{\cdot}30P_2S_5$ composition, the ambient temperature conductivity of the glass–ceramics is higher than that of $80Li_2S{\cdot}20P_2S_5$ glass–ceramic. The conductivity value of the $70Li_2S{\cdot}30P_2S_5$ glass–ceramic shown in Fig. 2 is 2.2×10^{-3} S cm^{-1} at room temperature, which was obtained after heating of the glass at 240 °C. The glass–ceramic obtained by heating at 360 °C exhibited the highest conductivity of 3.2×10^{-3} S cm^{-1} and the lowest activation energy of 12 kJ mol^{-1} for conduction. The reaction product obtained by solid-state reaction of 70 mol.%Li_2S and 30 mol.%P_2S_5 at 700 °C showed much lower conductivity of about 10^{-8} S cm^{-1}.

Precipitated crystals in the $70Li_2S{\cdot}30P_2S_5$ glass–ceramic were examined by use of X-ray diffraction measurements. In the glass–ceramics heated at 240 and 360 °C, a highly ion conductive new crystalline phase [14], which is not obtained by solid-state reaction, was formed. The highest conductivity obtained at the heat treatment of 360 °C would be caused by both the precipitation of the new crystalline phase and the increase in crystallinity of the phase. The $Li_4P_2S_6$ crystal with lower conductivity was mainly present in the case of the sample obtained by solid-state reaction. Thus, the superionic new crystalline phase was precipitated as a metastable phase in the case of crystallization of glass. The superionic metastable phase is responsible for the high conductivity and low activation energy for conduction of the $70Li_2S{\cdot}30P_2S_5$ glass–ceramic.

3.2. Construction of all-solid-state cells with a variety of active materials

The Li_2S–P_2S_5 glass–ceramics with ambient temperature conductivity of 10^{-3} S cm^{-1} was used as a solid electrolyte for all-solid-state cells of three-layered powder compressed pellets. The first layer was a negative electrode, e.g. an indium foil. The second layer was the glass–ceramics as an electrolyte. The third layer was a positive electrode, e.g., composite materials containing $LiCoO_2$. In order to achieve smooth electrochemical reaction in the cell, we prepared the composite positive electrode composed of three kinds of powders: the active materials like $LiCoO_2$, the solid electrolyte powder of Li_2S–P_2S_5 glass–ceramics providing lithium ion conduction path, and the electronic conducting materials like acetylene black providing electron conduction path. The composite positive electrode consisting of $LiCoO_2$, the $80Li_2S{\cdot}20P_2S_5$ glass–ceramic and acetylene-black powders with a weight ratio of 20:30:3 was used for a typical all-solid-state cell as an example [8,11]. This cell was charged and discharged under a constant current density of 64 μA cm^{-2} at room temperature in Ar atmosphere. Although an irreversible capacity was initially observed at the first few cycles, the all-solid-state cell maintained the reversible capacity of about 100 mAh g^{-1} and the charge–discharge efficiency of 100% (no irreversible capacity) for 500 cycles.

Fig. 3 shows charge–discharge curves at the 300th cycle for all-solid-state cells In or In–Li alloy/$LiCoO_2$, $Li_{4/3}Ti_{5/3}O_4$, or

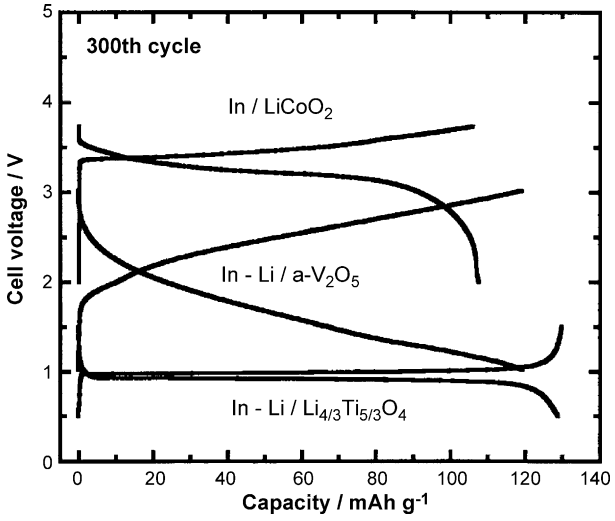

Fig. 3. Charge–discharge curves at the 300th cycle for all-solid-state cells In or In–Li alloy/$LiCoO_2$, $Li_{4/3}Ti_{5/3}O_4$, or amorphous V_2O_5.

amorphous V_2O_5. The $80Li_2S{\cdot}20P_2S_5$ glass–ceramic was used as a solid electrolyte. The electrochemical measurements were carried out at room temperature under a constant current density of 64 $\mu A\,cm^{-2}$. In spite of the 300th cycle data, high capacities and 100% efficiency are observed in the charge–discharge performance of all the cells with various electrode materials. The cells show different voltage plateaux based on the combination of electrode materials. The glass–ceramic electrolytes are compatible with various positive electrode materials for all-solid-state cells with excellent cyclability.

Much attention has also been devoted to develop negative electrode materials instead of conventional graphite in order to realize lithium secondary batteries with higher energy density. Tin-oxide-based glasses [19,20] were reported to work as a negative electrode material with high capacity in lithium ion cells. The cell performance of SnO-based glasses exhibited larger reversible capacity than the corresponding crystalline material [21]. We have also developed a series of SnO-based borate, phosphate, and borophosphate glasses [22,23] and found that the capacity of the cells using these active materials depended on the composition of glasses, and was closely related to local structure of the glasses.

Very recently, the $SnS–P_2S_5$ glassy materials were synthesized by mechanical milling and applied as an electrode to all-solid-state cells with the $Li_2S–P_2S_5$ solid electrolyte [24]. Because of using a common P_2S_5 component, a continuous sulfide network between electrode and electrolyte was formed in the cells.

Fig. 4 shows the first charge–discharge curves of all-solid-state cells of Li–In/$80SnS{\cdot}20P_2S_5$ and of Li–In/SnS. The $80Li_2S{\cdot}20P_2S_5$ glass–ceramic was used as an electrolyte in these cells. The charge–discharge measurements were carried out at a current density of 64 $\mu A\,cm^{-2}$ at 25 °C. The ordinate on the left hand side denotes cell potential versus the Li–In counter electrode, and that on the right hand side denotes potential versus the Li electrode, which was calculated from the basis of the difference on the potential between Li–In and Li [7]. A charge corresponds to an insertion of lithium ions to the working electrode, while a discharge corresponds to an extraction of lithium ions from the working electrode. Two plateaux at around 1.3 and 0.5 V (versus Li) are observed on the charge curve and one plateau at around 0.5 V is observed on the discharge curve in both cells. The $SnS\text{-}P_2S_5$ amorphous materials prove to work as electrode materials for all-solid-state rechargeable lithium batteries. The charge–discharge capacities of the cell with the $80SnS{\cdot}20P_2S_5$ electrode are larger than those with the SnS electrode. The discharge capacity of the cell with the $80SnS{\cdot}20P_2S_5$ electrode (590 mAh g^{-1}) is 1.5 times as large as the capacity of conventional graphite electrodes used in commercialized lithium ion secondary batteries. The charge–discharge efficiency for the cell with the $80SnS{\cdot}20P_2S_5$ electrode (56%) is larger than that of the cell with SnS (43%). The addition of P_2S_5 as a network former component to SnS is concluded to enhance the reversible capacity of the cells.

The charge–discharge profiles with two-step of the cells with $SnS–P_2S_5$ electrodes are quite similar to those of the nonaqueous lithium cells with $SnO–P_2O_5$ electrodes [23]. On the basis of the mechanism of electrochemical lithium insertion to SnO-based glassy materials [20–22], the first plateau on the charge curve of the cell with the $80SnS{\cdot}20P_2S_5$ electrode in Fig. 4 is probably due to the formation of metallic Sn nanoparticles and $Li_2S–P_2S_5$ glassy matrix (irreversible process), and the second plateau is due to the formation of Li–Sn alloy domains (reversible process). The formation of the highly Li^+ conductive $Li_2S–P_2S_5$ matrix around Sn active particles easily provides a close electrode–electrolyte interface, where smooth electrochemical reaction would occur during charge–discharge cycle. On the other hand, the less conductive Li_2S matrix would be formed in the cell with the SnS electrode. The sulfide glassy matrix played an important role in not only preventing the aggregation of Sn domains but also endowing the electrode with high conductivity. Hence, the $80SnS{\cdot}20P_2S_5$ electrode exhibited better performance than the SnS electrode as shown in Fig. 4.

Fig. 5 shows the charge–discharge curves at the 50th cycle of the all-solid-state $80SnS{\cdot}20P_2S_5/LiCoO_2$ cell. The $80Li_2S{\cdot}20P_2S_5$ glass–ceramic electrolyte was used in the cells. The charge–discharge measurements were carried out at a

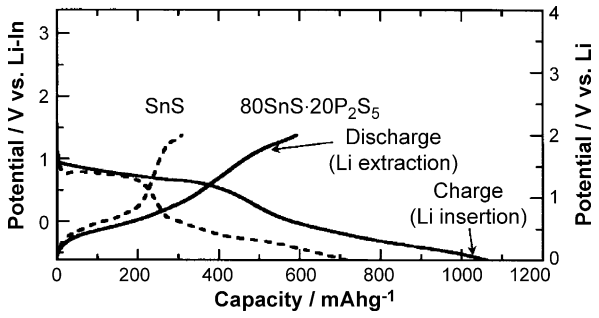

Fig. 4. The first charge–discharge curves of all-solid-state cells of Li–In/$80SnS{\cdot}20P_2S_5$ and of Li–In/SnS.

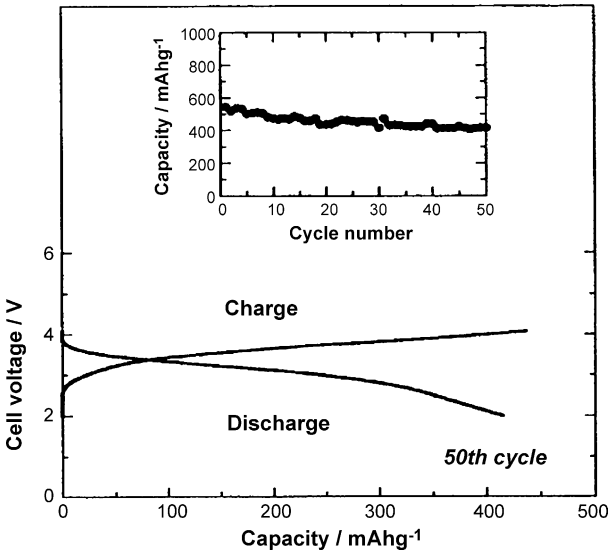

Fig. 5. The charge–discharge curves at the 50th cycle of the all-solid-state $80SnS{\cdot}20P_2S_5/LiCoO_2$ cell. The inset shows the cycling performance of the cell.

current density of 64 μA cm^{-2} in the potential range from 2 to 4 V. The cell capacity was calculated on the basis of the negative electrode. The charge–discharge plateaux of the cell are about 3.4 V. The inset shows the cycling performance of the cell. The reversible capacity gradually decreases and settled in over 400 mAh g^{-1} at the 50th cycle.

As a future development of all-solid-state cells, Souquet et al. proposed a glassy monolithic cell [25]: a common network former is used for the electrolyte and electrodes materials. The monolithic cell with a continuity for the lithium ion surrounding during its transfer from one electrode to the other would have a favorable feature of reducing the interfacial polarization during ion transfer. The all-solid-state cells with the combination of the SnS–P_2S_5 electrode and the Li_2S–P_2S_5 electrolyte is a first step for the realization of the monolithic cell.

3.3. Conductive additives in all-solid-state cells

The cells using liquid electrolytes usually exhibit favorable electrode–electrolyte interfaces, which can be realized only by soaking electrodes in liquid electrolytes. On the other hand, in the cells using solid electrolytes, electrode and electrolyte powders should be purposely contacted to form close solid–solid interfaces, where electrochemical reactions occur. In the solid-state cells, composite electrodes with a conductive additive are commonly used in order to form continuous electron conducting paths. Here, the effects of conductive additives in composite positive electrodes on charge–discharge behaviors of all-solid-state In/$LiCoO_2$ cells with the $80Li_2S{\cdot}20P_2S_5$ glass–ceramic electrolyte were investigated. Acetylene black (AB), vapor grown carbon fiber (VGCF), titanium nitride (TiN) and nickel (Ni) were used as conductive additives.

The morphologies of the conductive additives were examined using a field emission scanning electron microscope (FE-SEM). Fig. 6 shows FE-SEM photographs of AB, VGCF, TiN and Ni.

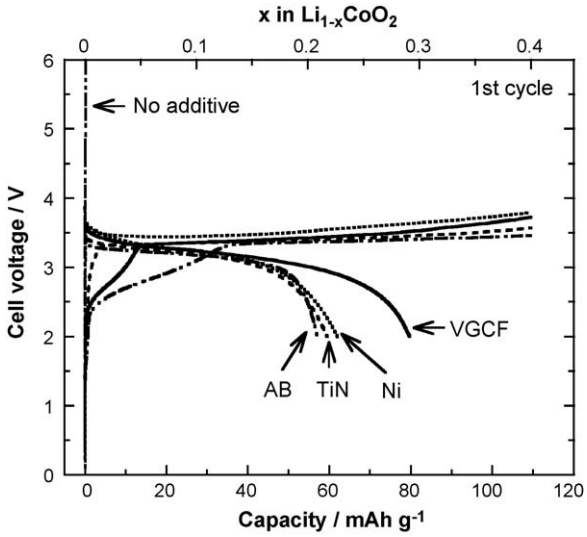

Fig. 7. The first charge and discharge curves of all-solid-state In/$LiCoO_2$ cells with various conductive additives of AB, VGCF, TiN and Ni.

AB is composed of aggregates with primary particles of about 15 nm in average size, whereas VGCF is composed of fibers of about 150 nm in average diameter and about 10 μm in average length. The average particle sizes of TiN and Ni are about 1.0 and 0.5 μm, respectively.

Using a composite positive electrode without a conductive additive ($LiCoO_2$:solid electrolyte = 40:60 (w/w)), the solid-state In/$LiCoO_2$ cell was assembled. The cell voltage rapidly reached 6 V in charging and the cell was not able to be discharged at a current density of 64 μA cm^{-2} (the charge–discharge curves are shown in Fig. 7). In this case, it is difficult to transport electrons in the composite positive electrode without a conductive additive. The addition of conductive additives is very important to achieve sufficient electronic conduction of composite positive electrodes.

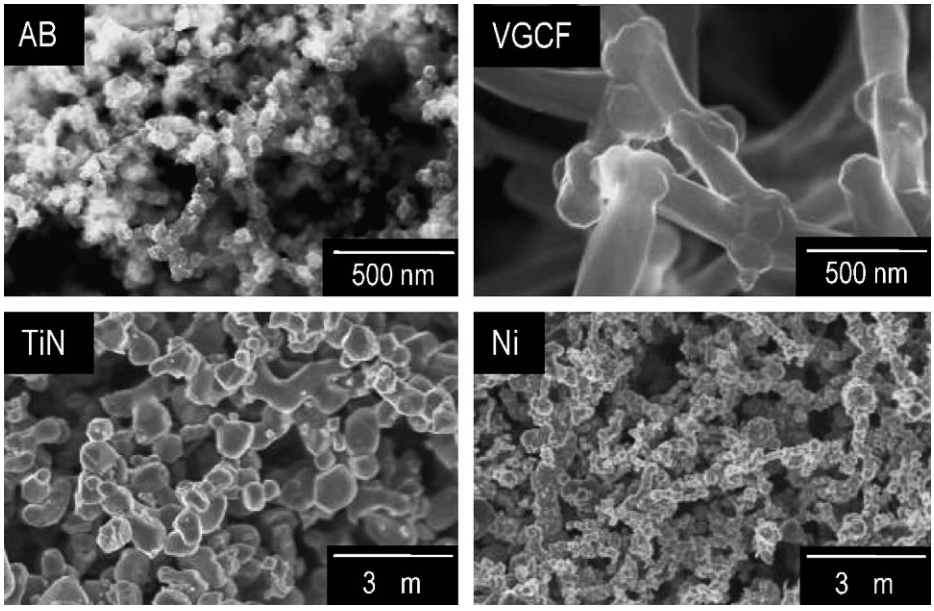

Fig. 6. FE-SEM photographs of AB, VGCF, TiN and Ni powders.

The additional amounts to endow composite positive electrode with sufficient electron conductivity were determined by ac impedance measurements for the model composite materials consisting of conductive additive and insulative sulfur [26]. Carbon materials AB and VGCF were more effective to decrease the resistivities of composite materials than TiN and Ni. Fig. 7 shows the first charge and discharge curves of all-solid-state In/$LiCoO_2$ cells with various conductive additives. The amounts of AB, VGCF, TiN and Ni added to the composite positive electrodes were respectively 6, 4, 60 and 40 wt.%, and a current density was 64 $\mu A\,cm^{-2}$. All cells with conductive additives work as rechargeable batteries at room temperature. Under a cut off voltage of 2.0 V, the cells with AB, TiN and Ni exhibit discharge capacities of about 60 mAh g^{-1}, while the cell with VGCF exhibits larger discharge capacities of about 80 mAh g^{-1}. All cells were charged up to $x = 0.40$ in $Li_{1-x}CoO_2$ (110 mAh g^{-1}) and discharged to 2.0 V until the second cycle, and then charge–discharge cycles were repeated between the maximum charge voltage of the second cycle and 2.0 V after the third cycle. The cell with VGCF maintained the discharge capacities of about 100 mAh g^{-1} and charge–discharge efficiencies of 100% up to the 300th cycle. On the other hand, discharge capacities of the cells with AB, TiN and Ni monotonically decreased with an increase in cycle number, although charge–discharge efficiencies of 100% were obtained. At the 30th cycle, discharge capacities of the cells with AB, TiN and Ni were respectively about 70, 50 and 60 mAh g^{-1}. The fact that the cells with AB and VGCF exhibited larger discharge capacities than those with TiN and Ni suggests that the carbon materials would be suitable to carry out reversible electrochemical reactions at solid–solid interfaces in the composite positive electrodes as compared with TiN and Ni.

Cell performances under high current densities over 1 mA cm^{-2} were examined for all-solid-state cells with carbon conductive additives. Fig. 8 shows the first charge and discharge curves of all-solid-state In/$LiCoO_2$ cells with AB and VGCF. The amounts of AB and VGCF added to the composite positive electrodes were respectively 6 and 4 wt.%, and a current density was 1280 $\mu A\,cm^{-2}$. The cells with AB and VGCF are charged and discharged even at a current density over 1 mA cm^{-2}, although the drops of the discharge potentials are observed. The cells with AB and VGCF exhibit discharge capacities of about 40 and 70 mAh g^{-1} under a cut off voltage of 1.5 V, respectively. The cell with AB shows a lower discharge plateau and a smaller discharge capacity than the cell with VGCF, suggesting that an overpotential observed in the cell with AB is larger than that in the cell with VGCF. Both cells were charged up to $x = 0.40$ in $Li_{1-x}CoO_2$ (110 mAh g^{-1}) and discharged to 1.5 V until the second cycle, and then charge–discharge cycles were repeated between the maximum charge voltage of the second cycle and 1.5 V after the third cycle. After the third cycle, discharge capacities of both cells monotonically decreased with an increase in cycle number, although charge–discharge efficiencies of about 100% were obtained. The discharge capacities of the cells with AB and VGCF at the 50th cycle were about 10 and 40 mAh g^{-1}, respectively, and the cell with VGCF kept larger discharge capacities during 50 cycles than the cell with AB [27]. The difference in the cycling performance for the cells with AB and VGCF would be closely related to the morphologies of conductive additives in composite positive electrodes. AB with nano-ordered primary particles would make contact with $LiCoO_2$ at the nanodimensional level. However, it is difficult to homogeneously disperse AB in the composite electrodes by dry-mixing because AB is easy to aggregate by itself. On the other hand, VGCF would make contact with $LiCoO_2$ at multiple points along submicron-ordered fibers. Since it is easy for VGCF to form a continuous electron conducting path within an electrode, the overpotential in the cell with VGCF was smaller than that with AB. Therefore, the cell with VGCF showed larger discharge capacity during 50 cycles than the cell with AB. The design of continuous electron conducting paths from the point of view of morphology for conductive additives is important to enhance cell performances of all-solid-state lithium secondary batteries. Fibrous VGCF is a promising conductive additive suitable for all-solid-state batteries.

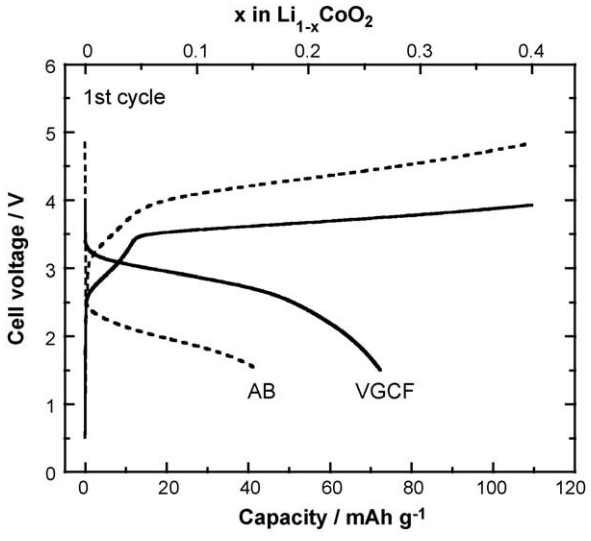

Fig. 8. The first charge and discharge curves of all-solid-state In/$LiCoO_2$ cells with AB and VGCF. The current density was 1280 $\mu A\,cm^{-2}$.

Acknowledgment

This work was partly supported by the Grant-in-Aids No. 11229204 (Priority Areas) and No. 15360350 (Section (B)) for Scientific Research from the Ministry of Education, Culture, Sports, Science, and Technology of Japan.

References

[1] C. Julien, G.-A. Nazri, Solid State Batteries: Materials Design and Optimization, Kluwer Academic Publishers, Boston, 1994, p. 579.
[2] J.-M. Tarascon, M. Armand, Nature 414 (2001) 359.
[3] J.B. Bates, Electron. Eng. 69 (1997) 63.
[4] B.J. Neudecker, N.J. Dudney, J.B. Bates, J. Electrochem. Soc. 147 (2000) 517.
[5] M. Tatsumisago, Solid State Ionics 175 (2004) 13.
[6] K. Iwamoto, N. Aotani, K. Takada, S. Kondo, Solid State Ionics 70/71 (1994) 658.

[7] K. Takada, N. Aotani, K. Iwamoto, S. Kondo, Solid State Ionics 86–88 (1996) 877.
[8] R. Komiya, A. Hayashi, H. Morimoto, M. Tatsumisago, T. Minami, Solid State Ionics 140 (2001) 83.
[9] A. Hayashi, R. Komiya, M. Tatsumisago, T. Minami, Solid State Ionics 152–153 (2002) 285.
[10] N. Machida, H. Maeda, H. Peng, T. Shigematsu, J. Electrochem. Soc. 149 (2002) A688.
[11] F. Mizuno, S. Hama, A. Hayashi, K. Tadanaga, T. Minami, M. Tatsumisago, Chem. Lett. (2002) 1244.
[12] K. Takada, T. Inada, A. Kajiyama, H. Sasaki, S. Kondo, M. Watanabe, M. Murayama, R. Kanno, Solid State Ionics 158 (2003) 269.
[13] A. Hayashi, S. Hama, T. Minami, M. Tatsumisago, Electrochem. Commun. 5 (2003) 111.
[14] F. Mizuno, A. Hayashi, K. Tadanaga, M. Tatsumisago, Adv. Mater. 17 (2005) 918.
[15] M. Tatsumisago, T. Minami, Mater. Chem. Phys. 18 (1987) 1.
[16] A. Hayashi, M. Tatsumisago, T. Minami, J. Electrochem. Soc. 146 (1999) 3472.
[17] R. Kanno, M. Murayama, J. Electrochem. Soc. 148 (2001) A742.
[18] M. Murayama, N. Sonoyama, R. Kanno, Solid State Ionics 170 (2004) 173.
[19] Y. Idota, T. Kubota, A. Matsufuji, Y. Maekawa, T. Miyasaka, Science 276 (1997) 1395.
[20] I.A. Courtney, J.R. Dahn, J. Electrochem. Soc. 144 (1997) 2943.
[21] Y.W. Xiao, J.Y. Lee, A.S. Yu, Z.L. Liu, J. Electrochem. Soc. 146 (1999) 3623.
[22] A. Hayashi, M. Nakai, M. Tatsumisago, T. Minami, M. Katada, J. Electrochem. Soc. 150 (2003) A582.
[23] A. Hayashi, T. Konishi, M. Nakai, H. Morimoto, K. Tadanaga, T. Minami, M. Tatsumisago, J. Ceram. Soc. Jpn. 112 (2004) S695.
[24] A. Hayashi, T. Konishi, K. Tadanaga, T. Minami, M. Tatsumisago, J. Power Sources 146 (2005) 496.
[25] J.L. Souquet, M. Duclot, Solid State Ionics 148 (2002) 375.
[26] F. Mizuno, A. Hayashi, K. Tadanaga, M. Tatsumisago, J. Electrochem. Soc. 152 (2005) A1499.
[27] F. Mizuno, A. Hayashi, K. Tadanaga, M. Tatsumisago, J. Power Sources 146 (2005) 711.